Iterative Linearization for Phasor-Defined Optimal Power Dispatch

Kyle Brady
Electrical Engineering and Computer Sciences
University of California, Berkeley
Berkeley, Calfornia 94720
Email: kwbrady@berkeley.edu

Alexandra von Meier
Electrical Engineering and Computer Sciences
University of California, Berkeley
Berkeley, Calfornia 94720
Email: vonmeier@berkeley.edu

***Abstract*—Optimal power flow (OPF) problems, which dispatch power targets to controllable generating units across a network, face non-convex constraints that arise from the physics of power flow. Describing those constraints in a way that allows the OPF problem to be solved with convex optimization techniques is an area of much academic and operational interest. It is a difficult problem, especially when considering unbalanced distribution systems. In this paper, we adapt an existing linearized power flow model that can then be used to solve OPF at the distribution level as a quadratic program with an iterative update technique. As an important benefit, the linearized model allows for the explicit inclusion of nodal voltage phasor values in both the OPF problem's objective and its constraints, which opens the door to the idea of phasor-based control (PBC) design. We show in simulations on the IEEE 13-node test feeder that our method quickly converges to a set of phasor targets that are sufficiently precise for use in operations at the distribution level.**

NOMENCLATURE

$\mathcal{N}$	Set of all nodes on the distribution feeder
$\mathcal{E}$	Set of all connecting line segments on the distribution feeder
$\mathcal{P}_{n,nm}; \mathcal{P}^k$	Subset of phases [A,B,C] present on node n or line nm; set of nodes with k phases present
V_n^ϕ	Complex-valued voltage phasor on phase ϕ of node n, magnitude given in per-unit RMS
E_n^ϕ	Squared per-unit RMS voltage magnitude on phase ϕ of node n.
θ_n^ϕ	Angle of the voltage phasor at phase ϕ of node n
p_n^ϕ	Per-unit active power demanded by the load on phase ϕ of node n
q_n^ϕ	Per-unit reactive power demanded by the load on phase ϕ of node n
$p_n^{g\phi}$	Per-unit active power generated by DER on phase ϕ of node n
$q_n^{g\phi}$	Per-unit reactive power generated by DER on phase ϕ of node n
$s_n^{R\phi}$	Per-unit apparent power rating of DER on phase ϕ of node n
I_{nm}^ϕ	Complex-valued phasor of current flowing from node n to node m on phase ϕ of line nm, magnitude in per-unit RMS
P_{nm}^ϕ	Per-unit active power flowing from node n to node m on phase ϕ of line nm
Q_{nm}^ϕ	Per-unit reactive power flowing from node n to node m on phase ϕ of line nm
P_{Lnm}^ϕ	Per-unit active power loss on phase ϕ of line nm
Q_{Lnm}^ϕ	Per-unit reactive power loss on phase ϕ of line nm
$R_{nm}^{\phi\psi}$	The resistive part of element ϕ, ψ of the 3x3 impedance matrix of the line connecting nodes n and m
$X_{nm}^{\phi\psi}$	The reactive part of element ϕ, ψ of the 3x3 impedance matrix of the line connecting nodes n and m
$Z_{nm}^{\phi\psi}$	The complex-valued impedance $R_{nm}^{\phi\psi}$ + $X_{nm}^{\phi\psi}$
$\mathbf{\Lambda}_n, \mathbf{\Lambda}_{nm}$	If $\Lambda_{n,nm}^\phi$ is a per-phase variable such as voltage, current, or power, the bold variable $\mathbf{\Lambda}_{n,nm}$ denotes the 3x1 vector $\begin{bmatrix}\Lambda_n^a & \Lambda_n^b & \Lambda_n^c\end{bmatrix}^T$ If $\Lambda_{n,nm}^{\phi\psi}$ is a cross-phase characteristic such as resistance, reactance, or impedance, the bold variable $\mathbf{\Lambda}_{n,nm}$ denotes the 3x3 matrix with elements $\Lambda_{nm}^{\phi\psi}$, where $\phi, \psi \in \mathcal{P}_{n,nm}$
c_{Kn}	$K \in \{Z, I, P\}$. Coefficients associated with the ZIP model components of a load at node n

I. INTRODUCTION

Recent advancements in the sensing technologies that can be deployed on the electric grid have opened up exciting new possibilities in the control of distributed energy resources (DERs). Categories of information that were previously only economically available on very high-voltage transmission networks can now be harnessed in the operations of medium-voltage distribution feeders and microgrids, areas where the penetration of DERs has increased dramatically over the past decade and necessitated a reassessment of traditional grid control schemes [1]. This expansion of sensing capabilities has enabled the consideration of fundamentally new strategies for dispatching DERs to achieve objectives that until very recently have not been possible at the distribution level.

This work was supported by U.S. Department of Energy
Award DE-EE0008008

978-1-7281-8192-9/21/$31.00

A significant development in distribution sensing is the ability to make phasor measurements at the medium voltage level. Carrying this out in a scalable and practical way has been enabled by the recent commercialization of phasor measurement units (PMUs) designed specifically for the distribution grid [2]. A chief characteristic of these distribution PMUs is an extremely high measurement precision, which is necessary to account for the small separation in voltage angle between adjacent nodes of a distribution grid in normal operation [3].

The "phasor" reported by a PMU expresses information about a voltage of the form $v(t) = V_{max}\cos(\omega t + \theta)$ in terms of a pair of values $V_{max}\angle\theta$ or $V_{rms}\angle\theta$. Implied in the definition of a phasor is that the frequency ω is a known constant, and the angle θ is referenced to a common clock. A great deal of information about the present operating state and stability of an electric network can be conveniently expressed in terms of phasors, and the ability to report and act on phasor information raises the possibility of re-casting some distribution-level control objectives in phasor terms. This idea is called phasor-based control (PBC); it was developed more fully in [4]. The PBC approach can be contrasted with more market-driven strategies for dispatching DERs, in which pricing and operational constraints combine to influence DER power contributions in ways that recall ISO strategies for managing generating resources on the transmission grid [5].

Phasor quantities are not commonly taken into explicit account when designing optimal power flow (OPF) objectives, particularly at the distribution level. As a family of problems, OPF is focused on minimizing a network-wide objective function given control over some set of loads and power generation resources. OPF problems are difficult, because faithful models of the power grid are generally nonlinear and non-convex. Over the years, proposed solutions to OPF problems have explored a number of approximations, decompositions, and other means of incorporating power flow models into more tractable convex optimization problems [6].

In designing a methodology that can be applied to phasor-based control of distribution systems, we propose incorporating an adaptation of a linearized power flow model into an iterative quadratic programming scheme, similar to the strategy described in [7], that makes additional use of a nonlinear power flow solver to refine the linear model that defines our QP's constraints. The quick convergence of this method to very precise values in simulation indicates that it will be worth further exploration in other environments.

For this work, "precision" is defined by the agreement of voltages generated by the solutions to the linearized OPF with values confirmed by the nonlinear solver to be feasible on the network. This is a necessary quality for any PBC strategy meant to function on distribution grids because of the very low impedances and small phase angle differences characteristic of those networks. As a motivating example: the IEEE 13-node test feeder has a voltage base of 2.4kV line-to-ground and contains a single-phase line with an impedance of magnitude $|Z| \approx 0.1\Omega$ [8]. If a set of phasor references generated by an OPF contains an error of magnitude Δ in the expected difference between the voltage phasors on either side of that line, that would translate into the attempted recruitment of 24Δ kiloAmps of erroneous actuation from DERs throughout the network. Even small Δ values would likely cause those DERs to saturate in an attempt to meet their targets and result in an extremely sub-optimal operating state for the feeder. The precision requirement of distribution-level, phasor-based OPF solvers will be a consistent theme in this work, and we will be returning to it numerically in the simulation results presented in Section IV.

This paper's contribution is the adaptation of a phasor-based, linear model for use in an iterative method of solving OPF and the demonstration of that method's applicability to a PBC scheme with extreme sensitivity to the OPF solution's precision. The paper will begin by presenting the structure of our OPF problem, which draws its constraints from the linear unbalanced power flow model (LUPFM) developed by [9], in Section II. In Section III, we will discuss our iterative solution methodology. Section IV will describe our simulation environment, objectives, and the modifications that were made to the IEEE 13-node test feeder. Section V will cover the results of those simulations, and Section VI will conclude the paper.

II. The OPF Formulation

For our OPF formulation, we choose an approximate linearized model of the power flow relations that can be used as constraints in a standard quadratic program (QP) to be solved at each iterative step of our method. The model is based on the "DistFlow" equations, originally introduced in 1989 [10] and then generalized to unbalanced, multiphase networks [11]. A later work introduced an additional relationship between voltage phasor angles and power flows that allows for the treatment of a phasor in its entirety within the structure of the model [9]. We present this latest form of the model, the linear, unbalanced power flow model (LUPFM), with minimal derivation in this section, but readers are encouraged to refer to [9] for further information. Several of the LUPFM's equations were adapted to allow for the use of the iterative method discussed in Section III and the inclusion of standard models of electric loads. We identify any equations which have been modified from the original forms of [9].

The LUPFM equations are linear with respect to the variables $\mathbf{E}_n$, $\boldsymbol{\theta}_n$, $\mathbf{p}_n^g$, $\mathbf{q}_n^g$, $\mathbf{P}_{nm}$, and $\mathbf{Q}_{nm}$. In order to maintain that linearity, other quantities such as current magnitudes and line power losses are replaced with estimated values. Those estimated values will be denoted by the superscript NL, as they will be generated by a nonlinear power flow solver for every OPF iteration.

A. The Linear Unbalanced Power Flow Model (LUPFM)

1) Real and reactive power balance: This constraint enforces the balance between power incoming over lines ln, power outgoing on lines nm, and the balance of load and generation at node n. Formally:

$\forall n \in \mathcal{N}$

$$\begin{aligned}\mathbf{p}_n - \mathbf{p}_n^g &= \sum_{ln\in\mathcal{E}} \mathbf{P}_{ln} - \sum_{nm\in\mathcal{E}} \mathbf{P}_{nm} - \sum_{nm\in\mathcal{E}} \mathbf{P}_{Lnm}^{NL} \\ \mathbf{q}_n - \mathbf{q}_n^g &= \sum_{ln\in\mathcal{E}} \mathbf{Q}_{ln} - \sum_{nm\in\mathcal{E}} \mathbf{Q}_{nm} - \sum_{nm\in\mathcal{E}} \mathbf{Q}_{Lnm}^{NL}\end{aligned} \tag{1}$$

The powers demanded by the loads $\mathbf{p}_n$ and $\mathbf{q}_n$ are 3x1 vectors of constants if all loads on the network are modeled as constant-P. To accommodate the classic ZIP model of electric loads [12], we alter the original LUPFM to replace them element-wise with (2):

$$\begin{aligned}p_n^\phi &= P_{\ell n}^\phi + I_{\ell Pn}^\phi(\frac{1}{2}|V_n^{\phi NL}| + \frac{1}{2|V_n^{\phi NL}|}E_n^\phi) + c_{Zn}^\phi \frac{R_n^{Ld}}{|Z_n^{Ld}|^2}E_n^\phi \\ q_n^\phi &= Q_{\ell n}^\phi + I_{\ell Qn}^\phi(\frac{1}{2}|V_n^{\phi NL}| + \frac{1}{2|V_n^{\phi NL}|}E_n^\phi) + c_{Zn}^\phi \frac{X_n^{Ld}}{|Z_n^{Ld}|^2}E_n^\phi\end{aligned} \tag{2}$$

where, in terms of per-unit nominal power demand $p_n^{\phi nom}$, $q_n^{\phi nom}$:

$$\begin{aligned}P_{\ell n}^\phi &= c_{Pn}p_n^{\phi nom} \qquad & Q_{\ell n}^\phi &= c_{Pn}q_n^{\phi nom} \\ I_{\ell Pn}^\phi &= c_{In}p_n^{\phi nom} \qquad & I_{\ell Qn}^\phi &= c_{In}q_n^{\phi nom}\end{aligned}$$

and R_n^{Ld}, X_n^{Ld}, Z_n^{Ld} are the resistance, reactance, and impedance of the load at nominal voltage and rated power. The expression for the constant-I component of the load was derived from a Taylor series in the variable E_n^ϕ.

2) Relation between voltage magnitudes and power flows: $\forall n, m \in \mathcal{N}; nm \in \mathcal{E}$

Let

$$\begin{aligned}\mathbf{M}_{nm} &= \mathbf{Re}(\mathbf{\Gamma}_m^{NL} \circ \mathbf{Z}_{nm}^*) \\ \mathbf{N}_{nm} &= \mathbf{Im}(\mathbf{\Gamma}_m^{NL} \circ \mathbf{Z}_{nm}^*) \\ \mathbf{H}_{nm} &= (\mathbf{Z}_{nm}\mathbf{I}_{nm}^{NL}) \circ (\mathbf{Z}_{nm}\mathbf{I}_{nm}^{NL})^*\end{aligned}$$

be the matrix equivalents of binomial coefficients of the multiplication $(\mathbf{V}_m + \mathbf{Z}_{nm}\mathbf{I}_{nm}^{NL}) \circ (\mathbf{V}_m + \mathbf{Z}_{nm}\mathbf{I}_{nm}^{NL})^*$. In the above, we define

$$\mathbf{\Gamma}_n^{NL} = \begin{bmatrix} 1 & \gamma_n^{ab} & \gamma_n^{ac} \\ \gamma_n^{ba} & 1 & \gamma_n^{bc} \\ \gamma_n^{ca} & \gamma_n^{cb} & 1 \end{bmatrix}$$

where $\gamma_n^{\phi\psi} = V_n^\phi / V_n^\psi$ is the complex-valued ratio of voltages on the phases ϕ and ψ of node n. Every element of the Γ_n^{NL} matrix is fixed, with the estimated voltage phasors being provided by the nonlinear solver at each iteration of the OPF, but we have dropped the NL superscript on the elements themselves for clarity of representation. The relation between the three-phase voltage magnitude at nodes n,m and power flows through each line nm can then be expressed as (3)

$$\mathbf{E}_n = \mathbf{E}_m + 2\mathbf{M}_{nm}\mathbf{P}_{nm} - 2\mathbf{N}_{nm}\mathbf{Q}_{nm} + \mathbf{H}_{nm} \tag{3}$$

3) Relation between voltage angles and power flows: $\forall n, m \in \mathcal{N}; nm \in \mathcal{E}$

$$|\mathbf{V}_m^{NL}| \circ |\mathbf{V}_n^{NL}| \circ (\boldsymbol{\theta}_n - \boldsymbol{\theta}_m) = -\mathbf{N}_{nm}\mathbf{P}_{nm} - \mathbf{M}_{nm}\mathbf{Q}_{nm} \tag{4}$$

where $\mathbf{M}_{nm}$ and $\mathbf{N}_{nm}$ are defined as above.

B. Other Constraints

1) Slack bus enforcement: $\mathbf{E}_{slack} \in \mathcal{N}$

$$\begin{aligned}\mathbf{E}_{slack} &= \begin{bmatrix}1 & 1 & 1\end{bmatrix}^T \\ \boldsymbol{\theta}_{slack} &= \begin{bmatrix}0 & -\frac{2\pi}{3} & \frac{2\pi}{3}\end{bmatrix}^T\end{aligned} \tag{5}$$

2) Voltage magnitude constraints: $\forall n \in \mathcal{N}, \phi \in \mathcal{P}_n$

$$\underline{\mathrm{V}}_{RMS}^2 \leq E_n^\phi \leq \overline{V}_{RMS}^2 \tag{6}$$

where $\underline{\mathrm{V}}_{RMS}$ and $\overline{V}_{RMS}$ are the lower and upper limits of the allowable RMS voltage magnitudes, respectively.

3) DER actuation constraints:

Limits on controllable DER follow the half-space approximation method in which a constraint on apparent power is transformed into an arbitrary number K of linear constraints on active and reactive power that can be used in our QP. These constraints are of the form

$\forall n \in \{s_n^\phi > 0,\ \phi \in \mathcal{P}_n\}$

$$\mathbf{\Psi}_{\cos} \circ \mathbf{p}_n^g + \mathbf{\Psi}_{\sin} \circ \mathbf{q}_n^g = \mathbf{s}_n^R \tag{7}$$

where

$$\begin{aligned}\mathbf{\Psi}_{\cos} &= \begin{bmatrix}\cos(\psi) & \cos(\psi) & \cos(\psi)\end{bmatrix}^T \\ \mathbf{\Psi}_{\sin} &= \begin{bmatrix}\sin(\psi) & \sin(\psi) & \sin(\psi)\end{bmatrix}^T \\ \psi &= \frac{2\pi k}{K} \quad for \ \ k = 0, 1, ..., K-1.\end{aligned}$$

The generation capacity sacrificed by this approximation can be made arbitrarily small at the expense of added constraints and increased computation time. When drawn in the space of active vs. reactive power, the difference in area between the set of linearized constraints and the original circular restriction on apparent power is less than 1% for $K \approx 20$ and 0.1% for $K \approx 60$ [9].

Ampacity constraints on distribution lines were not taken into account in this model, but could be included in future work with a similar half-space approximate treatment.

III. The Iterative Target Generation Methodology

The LUPFM has proved to be an effective tool for optimizing DER control over a network with respect to an arbitrary objective that can include both the magnitude and angle of nodal voltage phasors. However, because of the extreme sensitivity of power flows on a distribution network to minor changes in voltage, solving an OPF with linearized constraints can introduce an approximation error beyond what can be tolerated in control schemes with strict precision requirements. As mentioned in Section I, PBC in particular suffers from a danger of erroneous actuation being requested from DERs due to mismatch between linearized voltage phasors and voltage values that are achievable for those DERs on the physical network. Also, model approximations translate to a loss of ability to guarantee that any operating constraints included in the original OPF model are respected when DER action is taken on the physical feeder. The iterative solution

methodology described in this section addresses both these issues in generating PBC phasor targets, while generalizing to other use cases where high precision power flow solutions are desired.

For the first iteration of the method, the OPF problem is solved with constraints provided by the LUPFM as specified in Equations (2)-(7). We assume that no external sensor data is available at the process start, so the LUPFM is initialized with the values $\mathbf{V}_n^{NL} = \begin{bmatrix}1\angle 0 & 1\angle -120^\circ & 1\angle 120^\circ\end{bmatrix}^T$ and $\mathbf{I}_{nm}^{NL} = \mathbf{P}_{Lnm}^{NL} = \mathbf{Q}_{Lnm}^{NL} = \begin{bmatrix}0 & 0 & 0\end{bmatrix}^T$

The DER power dispatch $\mathbf{p}_n^g$, $\mathbf{q}_n^g$ generated by the solution of the QP OPF is then passed to a nonlinear power flow solver, which can be of any type so long as its model agrees with the line impedances and ZIP load modeling of the LUPFM. $\mathbf{p}_n^g$ and $\mathbf{q}_n^g$ are then included as negative, constant-P loads in the network model of the nonlinear solver, which uses them to generate magnitude and phase angle values for each of the network's nodal voltages and line currents.

At this point, the first iteration of the solution process is complete and the voltage phasors generated by the nonlinear solver can be compared to those of the QP OPF solution. If the difference between those two sets of voltage phasors is larger than a predetermined convergence threshold, the next iteration of the process begins. Each successive iteration re-initializes the LUPFM using the nodal voltage and line current values from the nonlinear solution of the previous iteration, i.e. $\mathbf{V}_n^{NL}$ and $\mathbf{I}_{nm}^{NL}$. These updates allow the successive linear approximations to approach a set of values $\mathbf{V}_n$, $\mathbf{p}_n^g$, and $\mathbf{q}_n^g$ that constitute an exact solution to the nonlinear power flow equations.

For all iterations following the first, an update is also made to the angular equation of the original LUPFM: the small-angle approximation is replaced with a more general Taylor series about the phase angle values returned by the nonlinear solver. Formally, Equation (4) of the original LUPFM is replaced by Equation (8):

$$|\mathbf{V}_m^{NL}| \circ |\mathbf{V}_n^{NL}| \circ \mathbf{\Delta}_{\sin\theta}^{NL} + |\mathbf{V}_m^{NL}| \circ |\mathbf{V}_n^{NL}| \circ \mathbf{\Delta}_{\cos\theta}^{NL} \circ [(\boldsymbol{\theta}_n - \boldsymbol{\theta}_m) - (\boldsymbol{\theta}_n^{NL} - \boldsymbol{\theta}_m^{NL})] = -\mathbf{N}_{nm}\mathbf{P}_{nm} - \mathbf{M}_{nm}\mathbf{Q}_{nm} \quad (8)$$

$$\mathbf{\Delta}_{\cos\theta}^{NL} = \begin{bmatrix}\cos(\theta_n^a - \theta_m^a) & \cos(\theta_n^b - \theta_n^b) & \cos(\theta_n^c - \theta_n^c)\end{bmatrix}^T,$$
$$\mathbf{\Delta}_{\sin\theta}^{NL} = \begin{bmatrix}\sin(\theta_n^a - \theta_m^a) & \sin(\theta_n^b - \theta_n^b) & \sin(\theta_n^c - \theta_n^c)\end{bmatrix}^T.$$

The superscript NL has been dropped from the individual angular elements of $\mathbf{\Delta}_{\cos\theta}^{NL}$ and $\mathbf{\Delta}_{\sin\theta}^{NL}$ to avoid clutter.

IV. The Simulation Environment

A. The 13-Node Feeder Model

The iterative method described in Section III was tested in simulation on a simplified version of the IEEE 13-node test feeder. While we expect that the technique would work equally well for the 13-node feeder as originally presented in [8], this simplified version has several modifications made to facilitate early programming efforts:

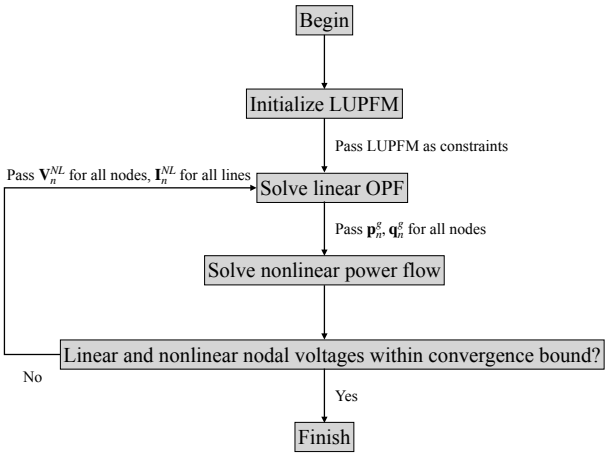

Fig. 1. The iterative update procedure for the LUPFM OPF and the nonlinear solver.

- The voltage regulator between Bus 632 and Bus 650 was replaced with a connecting line segment with impedance $Z_{650,632}^{\phi\phi} = .01 + .08j$ and $Z_{650,632}^{\phi\psi} = 2.5\cdot10^{-3} + 5\cdot10^{-3}j$ where $\phi \neq \psi$.
- The transformer XFM-1 connecting Bus 633 and Bus 634 was replaced with a line segment of configuration 601 and length 0.01mi. The switch connecting Bus 671 and Bus 692 was replaced with an identical segment.
- All delta-connected spot loads were replaced with wye-connected loads of the same magnitude. The ZIP model coefficients for each bus were kept consistent with [8].
- The distributed load on the line connecting Bus 632 and Bus 671 was replaced with a spot load of the same total value at Bus 632.
- All capacitor banks were removed from the system.
- DERs with capacity values of 0.025 per unit were added to each phase of nodes 675, 680, and 684, as in [9]. A large DER of capacity 0.2 per unit was added to Bus 632 to ensure available generation was sufficient to achieve operational objectives in the absence of approximation error.

B. OPF Objective I: Phasor Matching

For our first simulation, we chose a "phasor matching" objective for the OPF QP. In this use case, DER are dispatched so as to drive the voltage at a selected node $\mathbf{V}_i$ to a specific, externally provided phasor value $\mathbf{V}_{ext}$. The goal of the OPF solver in a phasor matching use case is to generate a feasible set of voltage phasor targets that can be sent to controllers at each node in the network. That target set will include a value for $\mathbf{V}_i$ that is as near as possible to $\mathbf{V}_{ext}$.

This ability to match voltage at a given node to a specified phasor value would be useful in distribution grid reconfiguration. If a grid contingency or maintenance requirement creates the need for connecting a distribution feeder to an adjacent network, this OPF formulation would

allow for the nodal voltage at the open tie switch to be matched to the value on the opposite side. PBC and the LUPFM are uniquely suited to this application because of the ability to match not only voltage magnitude but phase angle as well. With the phasors on either side of the open switch equalized immediately prior to closure, an out-of-phase closing is prevented and the potential for arcing reduced. The phasor matching objective is defined by Equation (9):

$\forall n \in \mathcal{N}; \forall nm \in \mathcal{E}$:

$$\min_{\mathbf{E}_n \boldsymbol{\theta}_n, \mathbf{p}^g_n, \mathbf{q}^g_n, \mathbf{P}_{nm}, \mathbf{Q}_{nm}} \quad (\mathbf{E}_{632} - \mathbf{E}_{ext})^2 + (\boldsymbol{\theta}_{632} - \boldsymbol{\theta}_{ext})^2 \tag{9}$$

C. OPF Objective II: Three-phase Balancing

For our second simulation, we chose an objective that attempts to balance voltages across phases A, B, and C of the feeder. The IEEE 13-node feeder has heavily unbalanced loading, and this is reflected in its unbalanced voltage profile even with the mitigating actions of transformer tap changes. Recruiting DER throughout the feeder to serve more load locally and to drive node voltages back toward balanced conditions can reduce losses, simplify feeder analysis, and improve the performance of three-phase loads. It is another application for which PBC is very well suited because of its ability to recruit both real and reactive power as needed.

We define perfectly balanced conditions at a 2- or 3-phase node as the state in which all voltage phasors have equal magnitude and there is 120° of angular separation between all phases $\phi \in \mathcal{P}_n$ Balanced feeder operation does not imply any restrictions on single-phase nodes.

The three-phase balancing objective is defined by Equation (10).

$\forall n \in \mathcal{N}; \forall nm \in \mathcal{E}; \forall \phi, \psi \in \mathcal{P}_n$:

$$\min_{\mathbf{E}_n, \boldsymbol{\theta}_n, \mathbf{p}^g_n, \mathbf{q}^g_n, \mathbf{P}_{nm}, \mathbf{Q}_{nm}} \quad \sum_{\forall n \in \mathcal{P}^3 \cup \mathcal{P}^2, \phi \neq \psi} (E^\phi_n - E^\psi_n)^2 + \sum_{\forall n \in \mathcal{P}^3 \cup \mathcal{P}^2, \phi \neq \psi} (\theta^\phi_n - \theta^\psi_n \pm \frac{2\pi}{3})^2 \tag{10}$$

V. Results

This section presents the results of the simulations discussed in Section III, all of which were carried out in Python. The cvxpy library and its default Operator Splitting QP Solver were used for the OPF stage of each iteration, and the nonlinear solver was implemented with the OpenDSSDirect library.

The LUPFM constraints on the QP were given as specified by Equations (2) through (8). The constraints were identical for both the phasor matching and three-phase balancing objectives. Because of the removal of voltage regulators on the network, the allowable range of feeder voltages was set wider than would be found on standard distribution feeders, with the lower bound $\underline{V}_{RMS} = 0.9$ and upper bound $\overline{V}_{RMS} = 1.1$ per unit.

The objectives for the use cases were given by Equation (9) for phasor matching and (10) for three-phase balancing.

A. Phasor Matching Results

For this test case, we select Bus 632 as our target node and $\mathbf{V}_{ext} = \begin{bmatrix} 0.975\angle 0^\circ & 0.975\angle -120^\circ & 0.975\angle 120^\circ \end{bmatrix}^T$ as the phasor target. Results are shown in Tables I and II.

TABLE I
Voltage Phasors at Bus 632, First Iteration

	Phase A	***Phase B***	***Phase C***
V^{lin}_{RMS}	0.9749999	.9750000	0.9750000
θ^{lin}	0.0000009	-120.0000050	120.0000120
V^{NL}_{RMS}	0.9691850	0.9753536	0.9761409
θ^{NL}_{RMS}	0.0502126	-120.1401553	120.1712758

TABLE II
Voltage Phasors at Bus 632, Fifth Iteration

	Phase A	***Phase B***	***Phase C***
V^{lin}_{RMS}	0.9750000	0.9750000	0.9750000
θ^{lin}	0.0000024	-120.0000036	120.0000049
V^{NL}_{RMS}	0.9749997	0.9750002	0.9750003
θ^{NL}_{RMS}	0.0000186	-120.0000077	120.0000039

From Table I, we can see that applying the optimal DER dispatch of the first iteration's OPF to the OpenDSS model results in a voltage phasor mismatch on the order of 10^{-3} per unit in magnitude and 0.1° in angle. These may seem like small errors, but when translated to PBC real and reactive power injections throughout the network they would result in significant discrepancies. In Table II, we see that five refinements to the LUPFM decrease the mismatch value to the order of 10^{-7} per unit in magnitude and 10^{-5} degrees in angle, which is within the acceptable error range of any reasonable OPF use case.

We see a similar error reduction at the system nodes whose voltage values were not included in the objective function. Figure 2 shows the decrease in error magnitude across the network over five iterations of the generation process. At each iterative step, we plot the maximum of the magnitude and angle differences between cvxpy- and OpenDSS-generated phasors at all nodes in the system. The sharp decrease in error over just a few iterations of the method speaks to its potential as a fast and accurate means of solving distribution-level OPF.

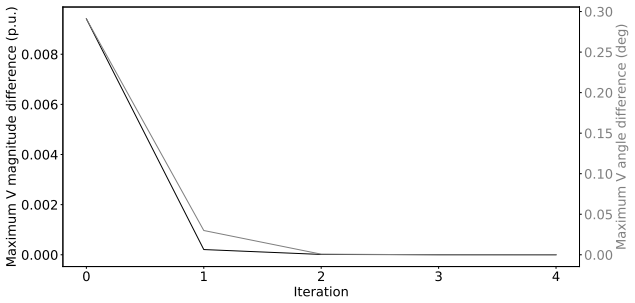

Fig. 2. Maximum difference between LUPFM OPF and OpenDSS phasor values with a phasor matching objective.

B. Three-Phase Balancing Results

Figure 3 shows that the maximum discrepancy between the LUPFM and OpenDSS phasors across the network decreases in a similar way for the three-phase voltage balancing objective as was seen in the previous subsection.

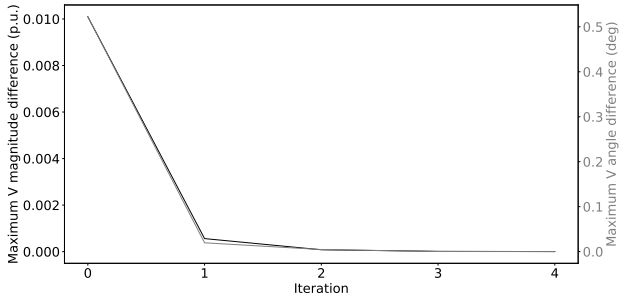

Fig. 3. Maximum difference between LUPFM OPF and OpenDSS phasor values with a voltage balancing objective.

Because the three-phase balancing objective involves many nodes, we take as our performance metric the agreement between the value of the objective function minimized by the LUPFM OPF and the value of that same objective calculated from the phasors generated by OpenDSS. The difference between the two decreases from $6.75 \cdot 10^{-3}$ for the first iteration to $6.31 \cdot 10^{-8}$ for the fifth. That progression is shown in Figure 4.

VI. Conclusion

The characteristics of distribution networks introduce complications for OPF solvers, particularly when they are expected to inform highly sensitive control strategies such as PBC.

This paper focused on achieving a level of precision sufficient for distribution operations when solving for optimal phasor targets with a QP. This was accomplished through the adaptation of a linearized power flow model to allow for its use in an iterative refinement scheme, where the selected model allows for the explicit treatment of voltage phasors on unbalanced distribution feeders. We demonstrated in simulation that our QP's set of optimal phasor values were

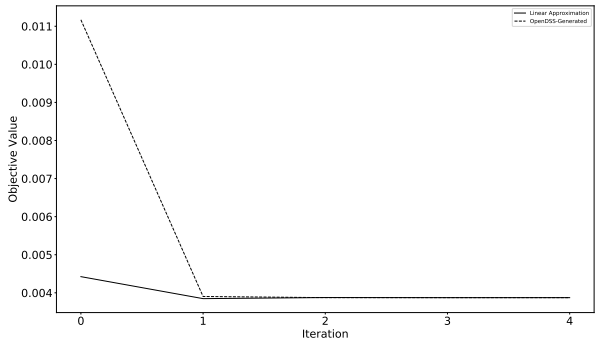

Fig. 4. Convergence of the three-phase balancing objective values achieved by the linear and nonlinear voltage profiles.

feasible based on their close agreement with a nonlinear power flow solution provided by OpenDSS.

Potential future work on this method includes demonstrating its application on more complicated feeder models, particularly those that include transformers and delta-connected loads. Another worthwhile area of exploration will be the use of this method in microgrid-specific cases and the consideration of the nonlinear solver's treatment of a slack bus in the absence of connection to a larger transmission grid.

References

[1] J. Romero Aguero and A. Khodaei, "Grid modernization, der integration utility business models - trends challenges," *IEEE Power and Energy Magazine*, vol. 16, no. 2, pp. 112–121, 2018.

[2] A. von Meier, E. Stewart, A. McEachern, M. Andersen, and L. Mehrmanesh, "Precision micro-synchrophasors for distribution systems: A summary of applications," *IEEE Transactions on Smart Grid*, vol. 8, no. 6, pp. 2926–2936, 2017.

[3] "micropmu datasheet," Power Standards Lab, 2019. [Online]. Available: https://www.powerstandards.com/product/micropmu/highlights/

[4] A. von Meier, E. Ratnam, K. Brady, K. Moffat, and J. Swartz, "Phasor-based control for scalable integration of variable energy resources," *Energies*, vol. 13, no. 1, p. 190, 2020.

[5] M. Faqiry, L. Edmonds, H. Zhang, A. Khodaei, and H. Wu, "Transactive-market-based operation of distributed electrical energy storage with grid constraints," *Energies*, vol. 10, p. 1891, 2017.

[6] M. Cain, R. O'Neill, and A. Castillo, "History of optimal power flow and formulations: Optimal power flow paper 1," Federal Energy Regulatory Commission, Tech. Rep., 12 2012.

[7] M. AlOwaifeer and A. P. S. Meliopoulos, "Centralized microgrid energy management system based on successive linearization," in *2018 North American Power Symposium (NAPS)*, 2018, pp. 1–6.

[8] W. H. Kersting, "Radial distribution test feeders," in *2001 IEEE Power Engineering Society Winter Meeting. Conference Proceedings (Cat. No.01CH37194)*, vol. 2, 2001, pp. 908–912 vol.2.

[9] M. Sankur, "Optimal control of commercial office battery systems, and grid integrated energy resources on distribution networks," Ph.D. dissertation, UC Berkeley, 2017, retrieved from https://escholarship.org/uc/item/5mb285r6.

[10] M. E. Baran and F. F. Wu, "Network reconfiguration in distribution systems for loss reduction and load balancing," *IEEE Transactions on Power Delivery*, vol. 4, no. 2, pp. 1401–1407, 1989.

[11] L. Gan and S. H. Low, "Convex relaxations and linear approximation for optimal power flow in multiphase radial networks," in *2014 Power Systems Computation Conference*, 2014, pp. 1–9.

[12] P. Kundur, N. Balu, and M. Lauby, *Power System Stability and Control*, ser. EPRI power system engineering series. McGraw-Hill Education, 1994. [Online]. Available: https://books.google.com/books?id=2cbvyf8Ly4AC